Sublimation-driven morphogenesis of Zen stones on ice surfaces

Nicolas Taberlet[a,1] and Nicolas Plihon[a]

[a]Laboratoire de Physique, Université Lyon, École Normale Supérieure (ENS) de Lyon, Université Claude Bernard, CNRS, F-69 342 Lyon, France

Edited by Eric Rignot, University of California, Irvine, CA, and approved August 31, 2021 (received for review May 17, 2021)

In this article, the formation of Zen stones on frozen lakes and the shape of the resulting pedestal are elucidated. Zen stones are natural structures in which a stone, initially resting on an ice surface, ends up balanced atop a narrow ice pedestal. We provide a physical explanation for their formation, sometimes believed to be caused by the melting of the ice. Instead, we show that slow surface sublimation is indeed the physical mechanism responsible for the differential ablation. Far from the stone, the sublimation rate is governed by the diffuse sunlight, while in its vicinity, the shade it creates inhibits the sublimation process. We reproduced the phenomenon in laboratory-scale experiments conducted in a lyophilizer and studied the dynamics of the morphogenesis. In this apparatus, which imposes controlled constant sublimation rate, a variety of model stones consisting of metal disks was used, which allows us to rule out the possible influence of the thermal conduction in the morphogenesis process. Instead, we show that the stone only acts as an umbrella whose shade hinders the sublimation, hence protecting the ice underneath, which leads to the formation of the pedestal. Numerical simulations, in which the local ablation rate of the surface depends solely on the visible portion of the sky, allow us to study the influence of the shape of the stone on the formation of the ice foot. Finally, we show that the far-infrared black-body irradiance of the stone itself leads to the formation of a depression surrounding the pedestal.

morphogenesis | differential ablation | sublimation

A wide variety of spectacular structures in which a stone or rock sits on a slender pedestal can be found in nature: hoodoos that consist of a hard stone protecting a narrow column of sedimentary rock from rain-induced erosion (1–3), mushroom rocks whose base is eroded by strong particle-laden winds (4), glacier tables for which a foot of ice resists melting due mostly to thermal insulation provided by a large rock (5–8),* and Zen stones on frozen lakes in which pebbles rest on delicate ice pedestals, as shown in Fig. 1 *A* and *B*. Although these structures differ in the nature of the erosion mechanisms, in timescales (from days for Zen stones to centuries for hoodoos), and in size dimension (from centimeters to tens of meters), the resulting shapes can be strikingly similar. Note also that micro- and nanofabrication processes, largely based upon differential etching of metal or semiconductor substrates, may lead to the formation of micrometer-sized optomechanical resonators with a geometry very similar to that of Zen stones (9, 10).

Most natural structures in which a stone sits on a pedestal are due to differential melting or mechanical abrasion. However, ice sublimation is known to drive a wide variety of morphologies in astrophysical bodies (11, 12). On Earth, sublimation-driven morphologies are rather scarce, with one well-known example being penitentes (13–15) encountered in the Andes and the Himalayas. However, numerous observations of sublimation-induced patterns have been made throughout the solar system, ranging from penitentes on Pluto (16) to landscape formation on Mars (17–19), Pluto (20), (1) Ceres (21), satellites of Jupiter (22–24), Saturn (25), and comets (26, 27).

In this article, we show that the morphogenesis of Zen stones is governed by differential sublimation rates of ice due to the shade provided by the stone, thus reporting a natural occurrence of sublimation-driven pattern formation on Earth. The Zen stones are reproduced in the laboratory (Fig. 1*C*) using an apparatus that allows for a controlled constant sublimation rate, while numerical simulations based on a geometrical numerical model recover the experimental results and allow us to study the influence of the shape of the stone on the formation of the ice pedestal (Fig. 1*D*).

Zen Stones in Nature

Zen stones on ice surfaces consist of natural phenomena in which a stone sits at the top of a slender ice pedestal (Fig. 1 *A* and *B*). Initially, the stone rests directly on a flat ice surface, but as the frozen surface is gradually eroded, the ice under the stone is protected by a mechanism that remained unexplained to date. Over time, the stone remains at its original altitude as the differential ablation induced by the umbrella effect carves an increasingly taller and thinner foot in the ice below, eventually causing the stone to fall off. Zen stones are rare in nature and predominantly found in the Small Sea of Lake Baikal, Russia, which is frozen for an average of 5 mo/y and where the ice layer typically reaches 1 m at the end of winter (28). The scarcity of the phenomenon stems from the rarity of thick, flat, snow-free layers of ice, which require long-standing cold and dry weather conditions. Weather records show that melting of the ice is virtually impossible and that, instead, the weather conditions (wind, temperature, and relative humidity) favor sublimation (*SI Appendix*, Figs. S1 and S2), which has long been known to be characteristic

Significance

Zen stones are fascinating natural structures consisting of a stone standing on a slender ice pedestal, whose origin had long been misunderstood. We demonstrate that they are caused by a variation in the sublimation rate of the surrounding ice, which leads to the slow formation of a pedestal, adding to the very few reports of sublimation-driven pattern formation. Understanding this process sheds light on other differential ablation processes encountered on ice surfaces, such as debris-covered glaciers, whose existence is threatened by global warming, and icy bodies in space. Indeed, NASA's Europa Lander project aims to seek biosignatures on Jupiter's ice-covered moon, on the surface of which differential sublimation may threaten the lander stability, and this needs to be fully understood.

Author contributions: N.T. designed research; N.T. performed research; N.T. and N.P. analyzed data; and N.T. and N.P. wrote the paper.

The authors declare no competing interest.

This article is a PNAS Direct Submission.

[1]To whom correspondence may be addressed. Email: nicolas.taberlet@ens-lyon.fr.

This article contains supporting information online at https://www.pnas.org/lookup/suppl/doi:10.1073/pnas.2109107118/-/DCSupplemental.

Published September 30, 2021.

*The similarities and differences between glacier tables and Zen stones are discussed in *Conclusion and Discussion*.

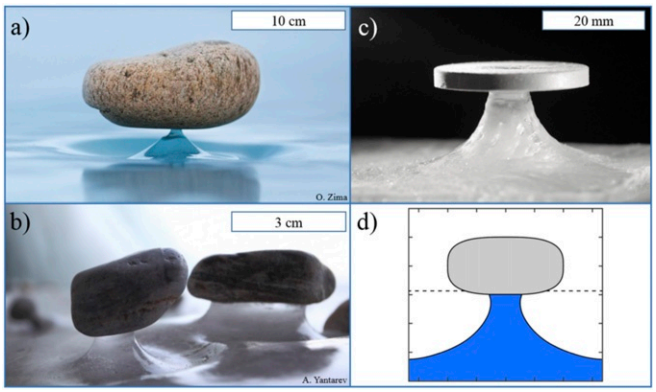

Fig. 1. Zen stones in nature, in the laboratory, and in numerical simulations. (*A*) A Zen stone on Lake Baikal (∼16-cm wide) showing a narrow ice pedestal. (*B*) Zen stones (∼3- to 5-cm wide) in a cave (Lake Baikal) with no direct sunlight. (*C*) A laboratory-scale experiment using a 30-mm aluminum disk initially resting on a flat ice surface and placed in a lyophilizer for 40 h. (*D*) A 2D numerical simulation of the phenomenon (the text has details). (*A*) Image credit: Instagram/zima_landscape. (*B*) Image credit: A. Yantarev (photographer).

of the Lake Baikal area (28). In particular, over a time interval spanning 7 wk prior to the date the photograph shown in Fig. 1*A* was taken, temperatures remained below 0°C, with an average daily maximum of −15.3°C and an average daily maximum relative humidity of 83%. From the average winter solar irradiance at the Small Sea and the latent heat of sublimation of water, one can estimate the ablation rate of an ice surface $u \sim 2$ mm/d, which gives a characteristic formation time of the pedestal $W/u \sim 40$ d for the stone of Fig. 1*A* (where W is the half-width of the stone, typically 8 cm in Fig. 1*A*). Sublimation is thus a slow surface process as well as an endothermic phase transition, which requires a constant flux of external energy, provided in nature by solar irradiance (11, 13, 14). Indeed, a net energy input of $60\mathrm{W/m^2}$ (or 5 MJ/m^2 per day) is required for the ice to sublimate (far from the stone) at the rate of 2 mm/d. At the latitude of Lake Baikal, in February or March, the irradiance reaches from 400 to 500 W/m^2 for typically 6 to 8 h. Assuming an emissivity of 0.95, the ice itself (at 260 K) radiates 246 W/m^2 back into the atmosphere. During the day, the net energy flux, therefore, largely exceeds what is needed to sublimate a few millimeters of ice, while the process stops at night. Note that this sublimation rate is only an average estimate and that the actual rate may depend on the exact optical properties of the ice [in particular, multiple scattering in white ice, which can considerably affect the energy balance (29)] as well as on the fluctuation of weather conditions. Regarding the energy balance of the stone itself, a pebble placed on the ice surface will receive the sunlight in place of the patch of ice it covers, possibly causing it to heat up. However, due to the good thermal contact with the ice, to the heat exchange with the cold ambient windy air, and to the far-infrared radiation (FIR) it emits back into the atmosphere, the temperature of the stone will remain very close to that of the ice. Therefore, the energy captured by the stone creates a deficit in the energy received by the ice. In simple terms, the stone acts as an umbrella under which the sublimation rate is greatly decreased.

One remarkable aspect of the ice pedestals is their axisymmetric shape, which might appear counterintuitive given that the position of the sun in the sky is preferentially oriented (20° above the horizon and ±60° from the south in the winter). This apparent contradiction is explained by the typical cloud cover during winter that scatters sunlight, rendering the irradiance more isotropic. The irradiance is maximum at the zenith (i.e., in the vertical direction), regardless of the actual position of the sun (*SI Appendix*, Fig. S3), and the luminous flux should be more isotropic than highly directional. Finally, although ablation appears to be caused by sublimation, it remains important to rule out other plausible mechanisms. First, direct sunlight might overheat the stone. However, the heat diffusion time of stones (computed from their size and thermal diffusivity) is of the order of several minutes, which implies that any overheating would quickly diffuse to the ice, causing it to melt rather than forming a pedestal. Second, wind-driven snow particle are known to cause mechanical erosion (30), but the clear and smooth natural pedestals show no indication of mechanical wear; also, the typical timescale of wind-driven erosion is far too long. Third, the melting temperature of water is known to vary with the ambient pressure. However, the phase diagram of water (*SI Appendix*, Fig. S2) reveals that it changes significant only for pressures above 10^7 Pa. The additional pressure of Zen stones on the ice does not exceed 10^5 Pa, far below the point where it could cause melting of the ice (which anyway, would not create a pedestal). Finally, ice is known to creep (i.e., undergo a slow plastic deformation) under high pressure (31). However, at −20°C, the typical deformation rate under a pressure of 10^5 Pa is only 10^{-9} s^{-1}, corresponding to a typical far too long deformation time of years. Note, however, that when a stone is initially placed on the ice surface, the stress would be locally high at the few points where the stone touches the ice. Given the high homologous temperature $T_{ice}/T_{melting} \simeq 0.95$, grain boundary migration (32, 33) could certainly occur initially, causing the ice to creep and the stone to slightly settle into the ice. As the actual surface of contact between the stone and the ice increases, the stress strongly decreases, and any deformation rapidly stops.

Laboratory Experiments

We have reproduced the formation of Zen stones in a laboratory-scale experimental setup. A metal disk (of radius $W = 15$ mm) representing the stone is placed at the surface of a block of ice sublimating in the chamber of a commercial lyophilizer (*Materials and Methods*). The external energy required to sublimate the ice originates from the IR black-body radiation of the outer walls of the vacuum chamber, which remains at room temperature (Fig. 2*A*). The ablation is then isotropic (in the absence of a stone) and mimics the relative isotropy of natural diffuse sunlight in overcast weather, with a sublimation rate of typically 8 to 10 mm/d (*Materials and Methods*).

Fig. 1*C* shows an artificial Zen stone obtained using a aluminum disk, initially resting on the ice surface, after 40 h in the lyophilizer, while Fig. 2 *B*–*D* shows the experimental results using three different metal disks (Movie S1 shows a time lapse of the experiment displayed in Fig. 2*D*). Clearly, our simplified setup is capable of qualitatively reproducing the formation of natural Zen stones. The evolution is shown over the first 28 h of operation since for longer times, the pedestals become too narrow and small asymmetries as well as mechanical vibrations often cause the disk to fall off. In nature, the process is slow (several weeks), which ensures a good thermal equilibrium of the stone. In our setup, however, due to the quasiabsence of air in the chamber, the stone can overheat (while remaining far below the melting temperature of ice). The excess energy accumulated in the stone then diffuses to the ice directly in contact with the stone, causing it to sublimate (*SI Appendix*, Fig. S4). In order to minimize this inconvenient side effect, thin metal disks made of polished metal were used, with higher reflectivity to IR radiations as compared with an unpolished surface. Fig. 2 *B* and *D* shows Zen stones obtained in the laboratory using aluminum and copper disks. The dynamics and the morphology of the two pedestals are very similar, although the thermal conductivity of Cu is nearly twice as large as that of Al. This result indicates that the thermal properties of the material are

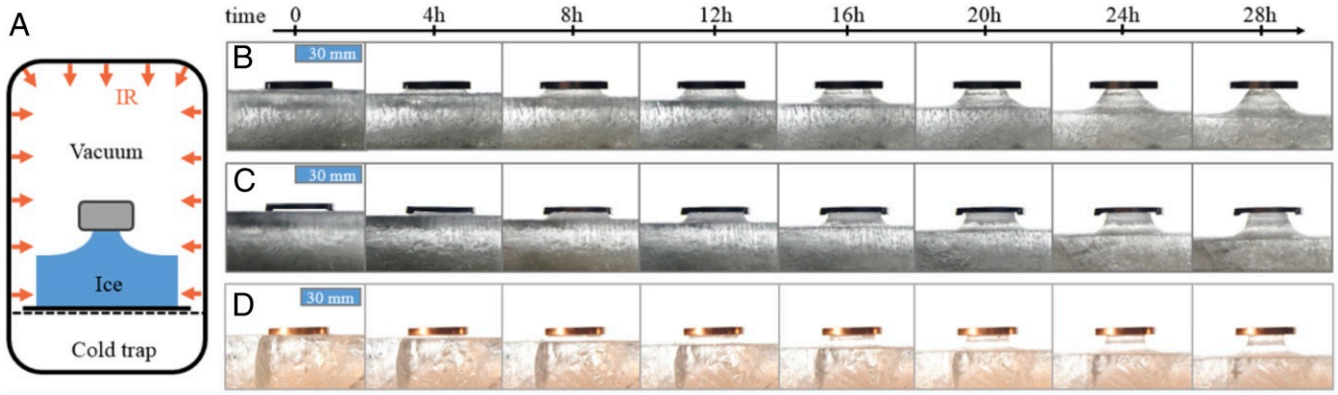

Fig. 2. Laboratory-scale formation of Zen stones on ice. (*A*) A sketch of the experimental setup. A metal disk rests on an initially flat block of ice in a lyophilizer. The energy required for the sublimation originates from the black-body radiation (in the far IR) of the vacuum chamber. Image sequences using (*B*) a 30-mm aluminum disk; (*C*) a grooved aluminum disk, which induces poor thermal conduction with the ice; and (*D*) a 30-mm copper disk are shown

not critical for the formation of Zen stones and that the main mechanism is the lack of radiation that the stone causes in its vicinity, leading to differential ice sublimation. Fig. 2*C* uses an aluminum disk, initially identical to that in Fig. 2*B*, in which a central groove is milled. Initially, the surface of contact between the disk and the ice is, therefore, extremely reduced, which limits its heat conduction. Although the exact morphologies of the pedestals are somewhat different, their overall shapes are very similar. The sole fact that a well-formed pedestal appears for the grooved disk is in itself an important result. Indeed, one plausible cause of differential ablation could have been that the sublimation was blocked by mechanical contact with the stone in the same way a thin plastic sheet can prevent a surface of water from evaporating. Instead, the milled-disk experiment indicates again that the stone acts as an umbrella, shielding the ice from external radiations (diffuse sunlight in nature and IR in the lyophilizer) and therefore, hindering the sublimation in its shade.

It is worth mentioning that two preparation protocols were used. In the original procedure, the "stone" was simply placed on the ice surface, whereas in a second protocol, the stone was initially embedded within the ice (when the ice block was built). In the former case, there were only initially very few contact points with the ice, and deformation could certainly occur. In the latter case, however, the weight of the stone was always evenly distributed, and the stress remained very low (a few pascals). Both protocols led to identical shapes for the pedestal, showing that over the long term, ice deformation or grain boundary diffusion does not play a role. Note that in theory, in latter stages when the pedestal becomes very narrow, the pressure exerted by the stone should diverge, possibly causing the ice to creep. However, as mentioned above, small perturbations and irregularities in the shape (both in the field and in our experiments) always caused the stone to fall off of its pedestal before this creep regime is ever reached.

Numerical Modeling

We have reproduced the formation of Zen stones in numerical simulations. As explained above, ablation is a surface process, and we model the surface of the ice as a series of connected points. For simplicity, the diffuse light is assumed to be isotropic, and the local luminous flux is proportional to the angle ϕ that the sky subtends at a given point (Fig. 3*A*). Our simulations compute the evolution of a two-dimensional (2D) ice surface, hypothesizing that the direction of sublimation is locally normal to the surface and that the rate of sublimation depends on the external radiative energy received (the computation of which is straightforward). The surface is simulated by an array

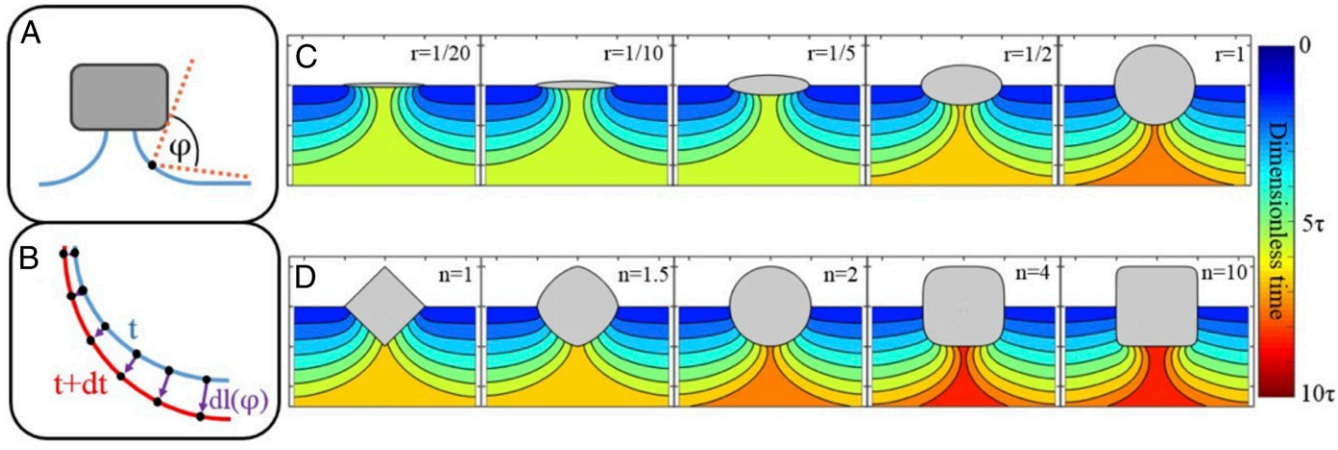

Fig. 3. The 2D numerical modeling of Zen stones. (*A*) A sketch showing the portion of sky, ϕ, visible from a position at the surface of the ice. (*B*) A sketch of the surface at two consecutive time steps. The ablation rate of the surface depends on the angle ϕ, and the sublimation is locally perpendicular to the surface. (*C*) The formation process of the pedestal for ellipses of varying height-to-width ratio *r*. The color scale indicates the dimensionless elapsed time from the initial flat surface. (*D*) The effect of the shape of the simulated stone on the morphology of the pedestal for an aspect ratio of one.

of n points $M_n(x_n, y_n)$ at time t, whose position at time $t + dt$ is computed (Fig. 3*B*). The half-width of the stone is set to $W = 1$, and the velocity of the sublimation front in the absence of the stone (i.e., for $\phi = 180°$) is set to $u = 1$; however, the choice of these numerical values has no effect on the resulting shape since our simulations rely on purely geometrical laws. The characteristic formation time $\tau = W/u$ is used as a scale for the computational time, and the integration time step dt is set to $10^{-4}\tau$.

Initially, the surface is flat, the first point is in contact with the stone, and each point is placed at a distance chosen to be 1/2,000th stone half-width. Due to the simple mathematical form chosen for the stone, its bottom is always curved and never truly flat. Therefore, in our numerical model, the stone is initially nested within the ice. The distance between the position of the nth point at times t and $t + dt$ is given by $dl_n = udt\phi_n/180°$. The direction of the displacement $\vec{dl}_n$ is chosen to be perpendicular to the two closest neighboring points [i.e., to the $(M_{n-1}M_{n+1})$ segment]. This procedure cannot be applied to the first point of the surface M_1, which is by definition in contact with the stone. Instead, the location of M_1 is always given by the point where the (M_2M_3) line intersects with the stone. Depending on the local slopes of the stones and the surface, it can happen that $\vec{dl}_2$ is such that $M_2(t + dt)$ rests within the stone. In that case, the surface is remeshed by simply relabeling the nth point as $n - 1$ and by removing the first point M_1.

This morphogenesis model, therefore, relies on geometrical arguments (inspired by the experimental results in the lyophilizer) rather than on overly complex thermodynamic processes and is intended to qualitatively reproduce the mechanisms. The shape of the stone is given by $\left(\frac{x}{W}\right)^n + \left(\frac{y}{H}\right)^n = 1$, where W and H are the half-width and half-height, respectively, and n is an exponent that determines the shape. Fig. 3*C* shows the temporal evolution of the ice surface for elliptical ($n = 2$) stones of varying aspect ratio $r = W/H$, while Fig. 3*D* shows the results obtained for stones of various shapes with an aspect ratio of one. As expected, the dynamics of the formation of the pedestal depend on the morphology of the stone. In all cases, a flat base produces an arched pedestal (Fig. 3*C*, $r = 1/20$ or Fig. 3*D*, $n = 10$), which corresponds to empirical observations in nature and in our model experiments, whereas a rounder base (Fig. 3*C*, $r = 1$ or Fig. 3*D*, $n = 1.5$) leads to moderate slopes. Moreover, the time required for the pedestal to reach the center of the stone (i.e., the lifetime of the Zen stone) varies with the exact shape of the stone. This simple numerical model thus shows that the shade provided by the stone provides favorable conditions for differential sublimation and leads to the formation of Zen stones for a variety of shapes.

Depression Surrounding the Pedestal

There is yet another striking feature of Zen stones that remains to be explained; the pedestal is always surrounded by a more or less pronounced depression (or dip or basin). This dip is clearly visible in Fig. 1*A*, somewhat less marked on the leftmost stone in Fig. 1*B*, and particularly evident in Fig. 4*E*, where its shape manifestly follows that of the stone.[†] In all observable cases, the dip is slightly larger than the typical size of the stone, while its exact morphology is clearly influenced by the shape of the stone. The very existence of a dip, relative to the average ice surface, indicates that the sublimation rate must be locally greater than that induced by the diffuse sunlight alone. The additional energy causing this local increase in the ablation rate can be attributed to the black-body radiation of the stone itself, which emits FIR, its temperature being in the in the range of -20 to $0°$C. While the umbrella effect is dominant regarding the overall dynamics of Zen stones, the FIR emitted by the stone is a necessary secondary effect, which creates the depression surrounding the pedestal. Fig. 4*A* shows a schematic of this mechanism, and Fig. 4*B* sketches the typical energy profiles of diffuse sunlight (blue) and of FIR (orange). Note that the irradiance of the sun in typically 100 times larger than that of the stone (Fig. 4*C*), but the values of the integrated energies are comparable (359 $\mathrm{W/m^2}$ for the solar energy vs. 259 $\mathrm{W/m^2}$ from the stone at 260 K). Moreover, the range of wavelengths differs strongly: 300 to 2,500 nm for sunlight vs. 5 to 50 μm for FIR. This difference has crucial implications since the extinction rate (i.e., the imaginary part of the refraction index) varies over 10 decades (Fig. 4*D*). Similarly, the absorption length of ice strongly depends on the wavelength (Fig. 4*D*): 10 km for a 400-nm radiation, meaning that the ice layer is then nearly transparent, vs. 10^{-5} m for a 10-μm radiation, meaning that the energy is absorbed within a 10-μm-thick layer, which facilitates surface sublimation of the ice. Note that the data in Fig. 4*D* correspond to pure ice; although multiple scattering in white ice may change the exact values of the extinction rate, the disparity remains huge, and the conclusions still hold. This colossal disparity implies that even if the FIR irradiance is two orders of magnitude lower than that of the diffuse sunlight, it can locally significantly increase the ablation rate. This explains why the depression mirrors the shape of the stone (Fig. 4*E*). Note also how the dip is deeper on the right side of the stone in Fig. 1*B* due to a more favorable orientation of the face on that side. The energy balance is, therefore, very subtle and varies during the day since the temperature of the stone and obviously, the amount of solar energy change from day to night. This is reminiscent of ablation processes of snow in forests for which the ablation rate can be either greater or less than surrounding open areas (38).

The additional effect of the FIR emitted by the stone can be implemented in the numerical simulations by adding an incoming energy to the external luminous flux (from the simulated sky). This added energy needs to be constant under a flat stone and should vanish away from it. The added contribution to the sublimation velocity is modeled as follows:

$$u_{IR} = u\left(1 - \mathrm{erf}\frac{x - W}{L}\right),$$

where x is the horizontal direction (from the center of the stone) and $L = W/5$ represents the characteristic length of IR illumination on the sides of the stone. As displayed in Fig. 4*F*, the added contribution in the FIR leads to the formation of a clear depression around the pedestal.

Conclusion and Discussion

Model experiments and numerical simulations were shown to reproduce the spectacular morphogenesis of the ice pedestal of Zen stones observed on frozen lakes on Earth. We have demonstrated that the formation is driven by differential sublimation of the ice, caused by the shade in the IR spectrum provided by the stone. A geometrical numerical model reproduces the experimental findings and helps us study the influence of the shape of the stone. Finally, we have shown that the dip surrounding the pedestal is caused by the FIR emitted by the stone itself, which enhance the overall sublimation rate in its vicinity.

As mentioned in the Introduction, very similar structures, known as glacier tables, may appear on low-altitude glaciers, where a rock initially sitting on the ice surface winds ups after a few days on top of an ice pedestal. These structures range from a few tens of centimeters up to a few meters. Although

[†]The photograph in Fig. 4*E* was taken by S. Tolstnev (https://facebook.com/tolstnev) in the Small Sea of Lake Baikal.

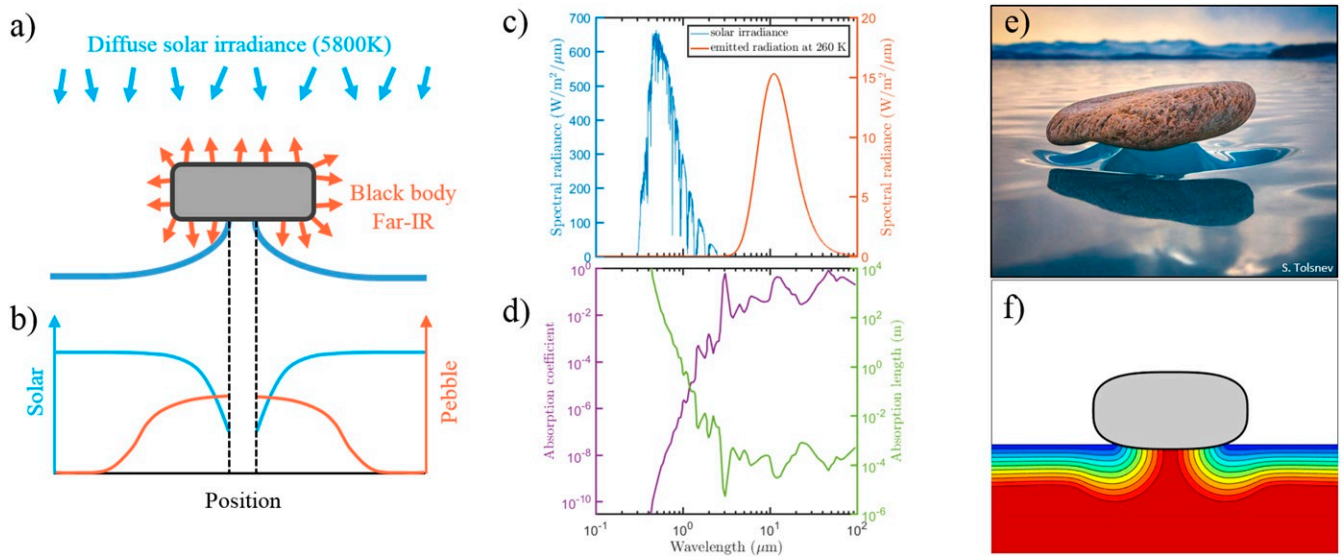

Fig. 4. Formation of the depression surrounding the ice pedestal. (*A*) A sketch showing the diffuse sunlight received by the ice and the black-body emission of the stone (of typical negative temperature close to 0°C) in the far-IR spectrum. (*B*) A sketch of the energy received per unit surface of the ice from diffuse sunlight (blue) and black-body radiation of the stone (orange). (*C*) The power spectrum of the solar irradiance at Lake Baikal on 1 February at solar noon generated using the Simple Model of the Atmospheric Radiative Transfer of Sunshine (34) (blue) and of the near-IR black-body emission from the stone at 260 K (orange). (*D*) The absorption coefficient (i.e., the imaginary part of the refraction index; purple) and the absorption length (green) of pure ice (35–37). (*E*) Zen stone on Lake Baikal, illustrating how the depression surrounding the ice foot mirrors the shape of the stone. (*E*) Image credit: Facebook/Stas Tolstnev. (*F*) Numerical modeling that includes the effect of the black-body emission leading to a dip around the pedestal.

they look similar to Zen stones, they are governed by different processes, and their shape and dynamics differ strongly. Glacier tables appear on low-altitude glaciers where the weather conditions cause the ice to melt instead of to sublimate. They form in warm air while the ice remains at 0°C, whereas Zen stones form in air that is colder (typically −30 to −10°C) than the ice (itself below 0°C).

Depending on their size and material as well as on the weather conditions, a stone or a pile of sand may either locally increase the melting rate, causing it to sink into the ice, or instead, hinder the melting process, leading to the formation of a glacier table or a dirt cone. In a recent study (8), some of us have shown that the differential melting of ice for glacier tables found on low-altitude alpine glaciers is dominantly caused by heat exchange with the surrounding air. The umbrella effect, which dominates the formation of Zen stones, is, therefore, only secondary for glacier tables encountered in the Alps. Instead, under these conditions, glacier tables form because the rock may act as a thermal insulator, and therefore, their thermal properties (conductivity and specific heat) are crucial. The conclusion is exactly opposite for Zen stones as demonstrated by our experiments performed using a variety of materials that lead to the same shape. Moreover, since heat conduction within glacier tables is crucial, there exists a minimum thickness (which depends on the material) below which the stone sinks deep into the ice instead of forming a table. This regime cannot be observed in the conditions where Zen stones form, and even a very thin stone will lead to an ice pedestal.

Materials and Methods

Experimental Protocol. The ice samples were prepared using purified and degassed water poured into a rectangular plastic container (15 × 15 cm, 5-cm deep). A 5-cm-thick block of Styrofoam was set to float at the surface of the water as it turned into ice (in a freezer at −20°C) in order to force the freezing front to travel from the bottom to the top, which helps in avoiding the formation of cracks as the water expands. The metal disks (at −20°C) were "glued" on the surface of the ice blocks using a few drops of liquid water. In order to maximize the reflection of IR radiations, the metal disks were polished using a buffing wheel. Ice samples were placed on a 1-cm-thick Styrofoam plate on the bottom metal shelf of a commercial lyophilizer (Christ Alpha 1–2 LDplus), and the pressure was gradually decreased over the course of 30 min in order to avoid the formation of quenching cracks within the ice. Specifically, while ice samples can withstand a rapid initial decrease from 1 bar to 10 mbar, a further decrease down to

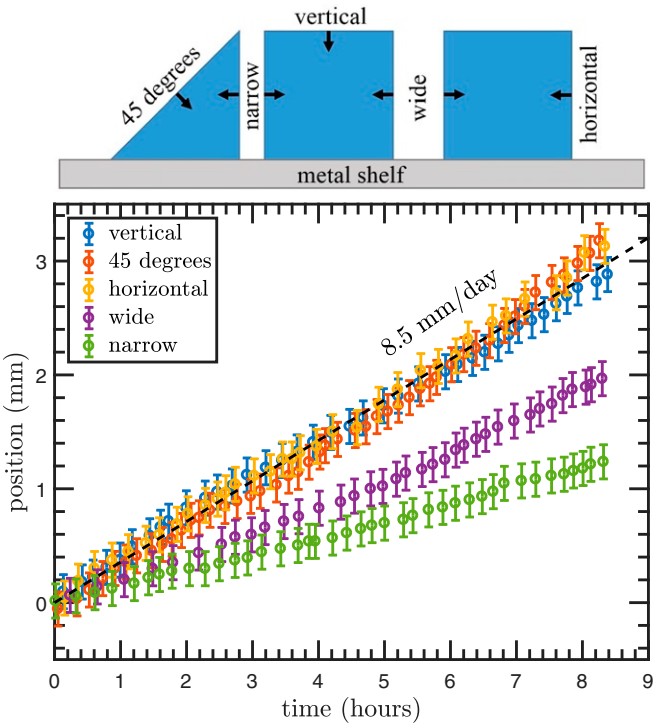

Fig. 5. Dynamic of sublimation of cubic blocks of ice (30 mm in length) in the lyophilizer (the sketch in *Upper*) measured from image processing.

the operating conditions of the lyophilizer (typically 50 μbar or 5 Pa) needs to be gradual.

Note that the temperature inside the lyophilizer depends note only on the pressure but also, on the cooling power of the device and on its ability to condensate vapor in its cold trap. In the experiments reported here, the temperature was around -45°C (i.e., below the temperatures observed at Lake Baikal in winter 2016). The profiles of the ice surface were imaged using a Nikon D5600 digital camera placed 2 m away in order to minimize parallax. The experiments were illuminated using a light-emitting diode (LED) panel (placed behind the vacuum chamber) and a regular lamp from the front, and the images were taken at regular 5-min intervals.

Sublimation Rate in the Lyophilizer. In order to demonstrate that the sublimation rate is both constant in time and independent of the orientation of the ice surface, three blocks were simultaneously placed in the lyophilizer. Fig. 5 shows that the sublimation rate remains constant over time (within error bars) and is identical for vertical, horizontal, and inclined surfaces, which indicates that the energy flux emitted by the surrounding vacuum chamber is isotropic and uniform. There is an initial spacing of 6 mm between the two first blocks and of 12 mm between the second and third blocks. For a narrow gap, the sublimation rate of the vertical surfaces is considerably reduced as the IR flux is hindered, and for a wider gap, the effect is still clearly visible, although less intense. Again, this shows that the source of energy required for the ice to sublimate is the black-body radiation of the acrylic vacuum chamber, which remains at room temperature.

The pressure within the chamber can be adjusted (typically in the 3- to 20-Pa range), which affects the sublimation rate. The data in Fig. 5 were obtained for 5 Pa and display a typical sublimation rate of 8.5 mm/d.

Data Availability. All study data are included in the article and/or supporting information.

ACKNOWLEDGMENTS. We thank the Fédération de Recherche Marie André Ampère and the Laboratoire de Physique at the ENS de Lyon for financial support.

1. R. W. Young, A. Young, *Sandstone Landforms (Lecture Notes in Physics*, Springer-Verlag, 1992).
2. J. Bruthans *et al*., Sandstone landforms shaped by negative feedback between stress and erosion. *Nat. Geosci.* **7**, 597–601 (2014).
3. A. V. Turkington, T. R. Paradise, Sandstone weathering: A century of research and innovation. *Geomorphology* **67**, 229–253 (2005).
4. H. M. Mashaal, E. S. Sallam, T. M. Khater, Mushroom rock, inselberg, and butte desert landforms (Gebel Aatrani, Egypt): Evidence of wind erosion. *Int. J. Earth Sci.* **109**, 1975–1976 (2020).
5. C. Smiraglia, G. Diolaiuti, "Epiglacial morphology" in *Encyclopedia of Snow, Ice and Glaciers*, V. P. Singh, P. Singh, U. K. Haritashya, Eds. (Springer, 2011), pp. 262–267.
6. M. Bouillette, Une superbe table des glaciers. *L'Astronomie* **47**, 201–202 (1933).
7. M. Bouillette, La fin d'une table des glaciers. *L'Astronomie* **48**, 89–91 (1934).
8. M. Hénot, N. Plihon, N. Taberlet, Onset of glacier tables. *Phys. Rev. Lett.* **127**, 108501 (2021).
9. B. Min *et al*., High-Q surface-plasmon-polariton whispering-gallery microcavity. *Nature* **457**, 455–458 (2009).
10. D. T. Nguyen *et al*., Ultrahigh q-frequency product for optomechanical disk resonators with a mechanical shield. *Appl. Phys. Lett.* **103**, 241112 (2013).
11. N. Mangold, Ice sublimation as a geomorphic process: A planetary perspective. *Geomorphology* **126**, 1–17 (2011).
12. J. Law, D. Van Dijk, Sublimation as a geomorphic process: A review. *Permafr. Periglac. Process.* **5**, 237–249 (1994).
13. V. Bergeron, C. Berger, M. D. Betterton, Controlled irradiative formation of penitentes. *Phys. Rev. Lett.* **96**, 098502 (2006).
14. P. Claudin, H. Jarry, G. Vignoles, M. Plapp, B. Andreotti, Physical processes causing the formation of penitentes. *Phys. Rev. E Stat. Nonlin. Soft Matter Phys.* **92**, 033015 (2015).
15. M. D. Betterton, Theory of structure formation in snowfields motivated by penitentes, suncups, and dirt cones. *Phys. Rev. E Stat. Nonlin. Soft Matter Phys.* **63**, 056129 (2001).
16. J. E. Moores, C. L. Smith, A. D. Toigo, S. D. Guzewich, Penitentes as the origin of the bladed terrain of Tartarus Dorsa on Pluto. *Nature* **541**, 188–190 (2017).
17. J. W. Head, D. R. Marchant, Cold-based mountain glaciers on mars: Western Arsia Mons. *Geology* **31**, 641 (2003).
18. M. Massé *et al*., Martian polar and circum-polar sulfate-bearing deposits: Sublimation tills derived from the north polar cap. *Icarus* **209**, 434–451 (2010).
19. L. E. Mc Keown, M. C. Bourke, J. N. McElwaine, Experiments on sublimating carbon dioxide ice and implications for contemporary surface processes on mars. *Sci. Rep.* **7**, 14181 (2017).
20. J. M. Moore *et al*., Sublimation as a landform-shaping process on Pluto. *Icarus* **287**, 320–333 (2017).
21. A. Nathues *et al*., Sublimation in bright spots on (1) Ceres. *Nature* **528**, 237–240 (2015).
22. A. D. Howard, J. M. Moore, Sublimation-driven erosion on Callisto: A landform simulation model test. *Geophys. Res. Lett.* **35**, L03203 (2008).
23. R. W. Carlson *et al*., "Europa's surface composition" in *Europa*, R. T. Pappalardo, W. B. McKinnon, K. K. Khurana, Eds. (University of Arizona Press, Tucson, AZ, 2009), pp. 283–327.
24. Europa Lander Mission Concept Team, "Europa lander mission, d-97 667" (Tech. Rep. NNN16D011T, NASA JPL, 2016).
25. J. R. Spencer, T. Denk, Formation of Iapetus' extreme albedo dichotomy by exogenically triggered thermal ice migration. *Science* **327**, 432–435 (2010).
26. D. T. Britt *et al*., The morphology and surface processes of Comet 19/P Borrelly. *Icarus* **167**, 45–53 (2004).
27. N. Thomas *et al*., Cometary science. The morphological diversity of comet 67P/Churyumov-Gerasimenko. *Science* **347**, aaa0440 (2015).
28. D. M. Livingstone, Ice break-up on southern Lake Baikal and its relationship to local and regional air temperatures in Siberia and to the North Atlantic Oscillation. *Limnol. Oceanogr.* **44**, 1486–1497 (1999).
29. P. C. Mullen, S. G. Warren, Theory of the optical properties of lake ice. *J. Geophys. Res. D Atmospheres* **93** (D7), 8403–8414 (1988).
30. R. V. Dietrich, Wind erosion by snow. *J. Glaciol.* **18**, 148–149 (1977).
31. D. J. Goodman, H. J. Frost, M. F. Ashby, The plasticity of polycrystalline ice. *Philos. Mag. A Phys. Condens. Matter Defects Mech. Prop.* **43**, 665–695 (1981).
32. M. Montagnat, P. Duval, Rate controlling processes in the creep of polar ice, influence of grain boundary migration associated with recrystallization. *Earth Planet. Sci. Lett.* **183**, 179–186 (2000).
33. O. B. Nasello, C. L. Di Prinzio, P. G. Guzmán, Temperature dependence of "pure" ice grain boundary mobility. *Acta Mater.* **53**, 4863–4869 (2005).
34. C. A. Gueymard, The smarts spectral irradiance model after 25 years: New developments and validation of reference spectra. *Sol. Energy* **187**, 233–253 (2019).
35. S. G. Warren, R. E. Brandt, Optical constants of ice from the ultraviolet to the microwave: A revised compilation. *J. Geophys. Res. D Atmospheres* **113** (D14), D14220 (2008).
36. G. Picard, Q. Libois, L. Arnaud, Refinement of the ice absorption spectrum in the visible using radiance profile measurements in Antarctic snow. *Cryosphere* **10**, 2655–2672 (2016).
37. S. G. Warren, Optical properties of ice and snow. *Philos. Trans. A Math. Phys. Eng. Sci.* **377**, 20180161 (2019).
38. J. D. Lundquist, S. E. Dickerson-Lange, J. A. Lutz, N. C. Cristea, Lower forest density enhances snow retention in regions with warmer winters: A global framework developed from plot-scale observations and modeling. *Water Resour. Res.* **49**, 6356–6370 (2013).